ARMY RESEARCH LABORATORY

CVD Synthesis and Characterization of Graphene Thin Films

by Matthew O'Brien and Barbara Nichols

ARL-TR-5047 **January 2010**

NOTICES

Disclaimers

The findings in this report are not to be construed as an official Department of the Army position unless so designated by other authorized documents.

Citation of manufacturer's or trade names does not constitute an official endorsement or approval of the use thereof.

Destroy this report when it is no longer needed. Do not return it to the originator.

Army Research Laboratory
Adelphi, MD 20783-1197

ARL-TR-5047 **January 2010**

CVD Synthesis and Characterization of Graphene Thin Films

Matthew O'Brien and Barbara Nichols
Sensors and Electron Devices Directorate, ARL

REPORT DOCUMENTATION PAGE

Form Approved
OMB No. 0704-0188

1. REPORT DATE *(DD-MM-YYYY)*	2. REPORT TYPE	3. DATES COVERED (From - To)
January 2010	Final	

4. TITLE AND SUBTITLE
CVD Synthesis and Characterization of Graphene Thin Films

5a. CONTRACT NUMBER

5b. GRANT NUMBER

5c. PROGRAM ELEMENT NUMBER

6. AUTHOR(S)
Matthew O'Brien and Barbara Nichols

5d. PROJECT NUMBER

5e. TASK NUMBER

5f. WORK UNIT NUMBER

7. PERFORMING ORGANIZATION NAME(S) AND ADDRESS(ES)
U.S. Army Research Laboratory
ATTN: RDRL-SER-L
2800 Powder Mill Road
Adelphi, MD 20783-1197

8. PERFORMING ORGANIZATION REPORT NUMBER
ARL-TR-5047

9. SPONSORING/MONITORING AGENCY NAME(S) AND ADDRESS(ES)

10. SPONSOR/MONITOR'S ACRONYM(S)

11. SPONSOR/MONITOR'S REPORT NUMBER(S)

12. DISTRIBUTION/AVAILABILITY STATEMENT
Approved for public release; distribution unlimited.

13. SUPPLEMENTARY NOTES

14. ABSTRACT
We demonstrated a method for producing high-quality, few-layer graphene over large areas via chemical vapor deposition (CVD). Graphene growth was achieved by the flow of methane and hydrogen gasses over a nickel thin film acting as catalyst at ambient pressure. Optimal growth conditions were found by varying the following parameters: methane flow rate, nickel film thickness, cooling rate, and temperature. A transfer process was developed through treatment with a nickel etchant solution to isolate the graphene for placement on an oxidized silicon substrate. Transfer methods are essential for effective optical contrast and atomic force microscopy measurements. Characterization was performed with optical microscopy, Raman spectroscopy, and atomic force microscopy to determine the number and quality of layers. Results have shown noticeable differences in Raman signals and optical color contrast between graphene and graphite, as well as distinctions between single-to-few- and multi-layer graphene.

15. SUBJECT TERMS
Graphene, chemical vapor deposition, raman

16. SECURITY CLASSIFICATION OF:			17. LIMITATION OF ABSTRACT	18. NUMBER OF PAGES	19a. NAME OF RESPONSIBLE PERSON
a. REPORT	b. ABSTRACT	c. THIS PAGE	UU	24	Barbara Nichols
Unclassified	Unclassified	Unclassified			19b. TELEPHONE NUMBER (*Include area code*) (301) 394-0602

Contents

List of Figures

List of Tables

INTENTIONALLY LEFT BLANK.

1. Background

As the thinnest material known, graphene would be easy to miss, but the buzz and intrigue about it on the nanotechnology radar screen is off the charts. Graphene is a one atom thick sheet of carbon atoms arranged in a honeycomb lattice that can essentially be thought of as a 2D material. Although graphene was only isolated as a single-layer substance in 2004 (*1*) and previously thought impossible to make, several related carbon allotropes have been known for some time (see figure 1) (*2*). Graphite can be thought of as a 3D stack of graphene layers held together by van der Waals interactions. Carbon nanotubes, another material having captured researchers fascination in the last two decades, can be fundamentally thought of as a sheet or sheets (depending on if they are single-walled or multi-walled carbon nanotubes) of graphene rolled up on itself into a 1D tube. The buckminsterfullerene, otherwise known as a buckyball or C_{60}, is a graphene sheet rolled up into the shape of a sphere that can be effectively considered 0D. Carbon covers a range of conformations and dimensions, properties and uses, with graphene already having begun to differentiate itself from related allotropes with much more yet to be discovered.

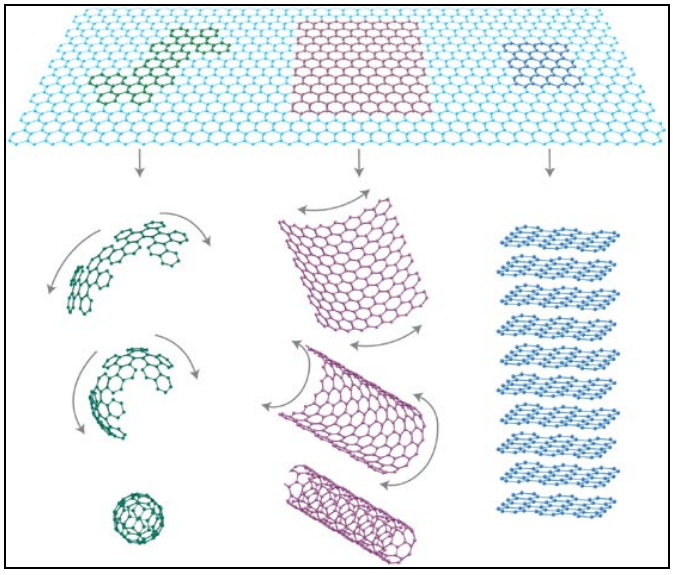

Figure 1. Graphene as the fundamental building block of (from left to right): buckyballs, carbon nanotubes, and graphite (figure taken from reference 2).

Graphene possesses a range of unique properties - an exciting electronic character, described as a zero-gap semiconductor (*3*), unparalleled strength (breaking strength ~40 N/m, Young's modulus ~1.0 TPa) (*13*), and record thermal conductivity (*14*). Charge carriers, described as massless Dirac fermions, exhibit ballistic movement across submicron distances approaching relativistic speeds, with intrinsic carrier mobilities up to 200,000 $cm^2 V^{-1} s^{-1}$ (*2, 4, 6*). In fact, graphene can

maintain current densities six orders of magnitude greater than that of copper (*7*). All of this can be achieved with little electronic noise (exhibiting little extraneous noise from outside sources), which is increasingly important as microelectronic devices continue to shrink in size (*1–3*). With thickness on the order of atoms, graphene has a high surface area-to-volume ratio while maintaining incredible flexibility. As additional layers are introduced, the structure becomes increasingly complex, resulting in more distinct and/or unique behavior. Depending on the number of layers, the magnitude of the electric field applied, and the edge orientation, the band gap of the material can be engineered to achieve a wide range of values (*1, 3–5*).

With all of those exciting characteristics, a wealth of potential applications is easy to envision ranging from single-electron transistors to enhanced composite materials. As the current generation of silicon-based devices reaches their fundamental minimum size limit in the coming years, graphene provides an opening to proceed even smaller. Since graphene remains conductive and stable at the molecular level, it is in a position to provide the next generation of low power electronics, such as graphene-based transistors as demonstrated by Ponomarenko, et al., (see figure 2) (*8–10*). Hurdles, such as achieving zero conductance due to the quantum Hall effect, must first be overcome before graphene-based nanoelectronics come to fruition, but it is exciting nonetheless (*1, 3, 4, 8–10*). Chemical and biological sensors are another promising direction, where molecules adsorbing onto the surface play the role of pseudo-dopants, producing a distinct and noticeable change in electrical conductivity. This change in conductivity should be sensitive enough to indicate the adsorption/desorption of individual molecules (including NO_2, NH_3, K, and OH) (*11, 12*). Graphene's 2D nature allows for a large array catchment area, while functionalization and tunability enables specifically tailored sensors to a variety of desired substances (*7, 11, 12*). One can imagine a new class of sensors – responding faster, more sensitive to minute concentrations at shorter exposure times, taking advantage of the lightweight and stiffness that this material provides. By capitalizing on graphene's unique electronic and structural properties, flexible electronics and transparent membranes, such as in the replacement of indium tin oxide (ITO) as an electrode in liquid crystal displays (LCD), organic light emitting diodes (LED), or photovoltaic devices, may also be possible (*7, 15, 16*). All of these potential applications offer promising possibilities towards helping the Soldier, in addition to a host of other Army applications left unmentioned or unimagined. Before their use can be realized, an understanding of graphene, its properties, and an optimal method for its fabrication must first be developed.

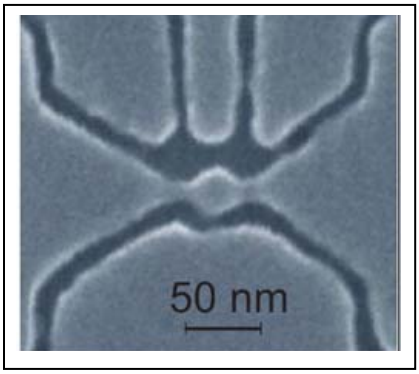

Figure 2. Graphene-based transistor (image taken from reference 8).

Currently there are several methods for production of graphene that vary in scale, structural consistency, ease of fabrication, and cost including: (1) microcleaving or micromechanical exfoliation of highly oriented pyrolitic graphite (HOPG), (2) chemical exfoliation from bulk graphite, and (3) thermal decomposition of silicon carbide (*7, 15–19*). The first method is the most commonly used for research and is how graphene was first isolated (*1*); however, it is limited to small areas providing little chance for successful scaling in the future for widespread use. For the second, the rigorous exfoliation and reduction processes can produce structural defects and poor interlayer contact resistance, making it impractical for device creation. The last method is limited by the difficulty of transferring sheets to alternative substrates, limiting their integration with CMOS fabrication (*7, 15–19*). Many of the aforementioned applications require uniformity of very few layers with significant coverage created in an affordable and scalable means, a description none of the above techniques entirely fits.

Chemical vapor deposition (CVD) is an attractive approach to graphene production due to its capability of producing large area deposition and the lack of intense mechanical and/or chemical treatments. For this method, a wafer with a thin transition metal film plays the role of catalyst. This substrate is placed in a heated furnace and is attached to a gas delivery system, which flows a gaseous carbon source downstream to the metalized wafer. It is believed that carbon is then adsorbed and absorbed into the metal surface at high temperatures, where it is then precipitated out in the lowest free energy state (graphene) during the cool down to room temperature (*15–20*). This report describes the CVD growth and characterization of graphene thin films. Various growth parameters were varied to determine the optimal fabrication conditions for graphene. A transfer process was employed to remove the graphene film from the metalized substrate and onto an oxidized silicon wafer. For purposes of this paper, the following conventions will be assumed with respect to number of layers *n*: few-layer graphene ($n < 5$), multi-layer graphene ($5 < n < 20$), and graphite ($n > 20$) (*21*).

2. Experimental Procedure

2.1 Substrate Preparation and Metal Deposition

Beginning with metal evaporation of different thicknesses, substrates were prepared for use in a CVD process. Nickel layers of 1000 Å, 2000 Å, and 3000 Å thickness were deposited via electron-beam evaporation (CHA e-Beam Vacuum Evaporator System) onto 4 in silicon wafers with 1 µm thermal silicon dioxide (SiO_2). The nickel thickness determines the amount of carbon that can be dissolved in solid solution and therefore will precipitate out. Adhesion of the nickel to the substrate surface was initially a problem, but was solved through the addition of a chromium layer approximately 10% of the nickel thickness. Because of the relatively low carbon solubility in chromium, the amount of additional carbon absorbed is negligible (*22*). Profilometry was used near the edge of the substrates where no nickel had been deposited to confirm the desired thicknesses within about 20–30 Å, which is sufficient since the relative thicknesses are orders of magnitude larger than this uncertainty.

To observe the effects of annealing on the nickel thin films, we put several substrates through a typical CVD process sequence (detailed in section 3.2) without the carbon source flowing at 1000 °C. Grain size and surface roughness measurements prior to and after annealing were performed on these samples via atomic force microscopy (AFM, Veeco Dimension V). These measurements give an indication of the surface topography and grain size of the subsequent graphene growth.

2.2 Chemical Vapor Deposition

We conducted CVD using a horizontal tube furnace at ambient pressure with argon, hydrogen, and methane flows. Three nickel film samples of different thicknesses were used in each run. On account of the large size of the tube being used and the uniformity of the temperature throughout the furnace, it is assumed that any differences due to position can be ignored. Several parameters were chosen for exploration (see table 1 for details).

Table 1. Experimental growth parameters.

Cooling Rate	5, 10, 25 °C/min
Nickel Thickness	1000, 2000, 3000 Å
Methane Flow	30, 60, 90 sccm
Temperature	900, 1000 °C

The synthesis process, as detailed in figure 3 with specific flow rates, begins with heating the substrates to the desired furnace setpoint temperature in an argon and hydrogen atmosphere. Once this temperature was achieved, a 20 min annealing step was conducted, allowing temperature stabilization and nickel grain growth. At the end of this period, growth was started by introducing methane, which acts as the carbon source. Duration of this "growth" phase was 10 min, and the end was signaled by reducing the heat source at the appropriate cooling rate and allowing the furnace to return to room temperature. With the greatest temperature decrease occurring immediately following the end of the "growth" stage, we focused on control of this temperature region (900–1000 °C to 500–600 °C). Cooling rates were measured in the first five to ten minutes with an in-tube thermocouple and altered from the natural furnace cooling rate (~25 °C/min) by programming a furnace ramp down rate (e.g., 5 or 10 °C/min). Once the tube temperature reached 500 °C, methane and hydrogen flows were stopped in favor of argon, with little presumed precipitation or growth occurring below this temperature.

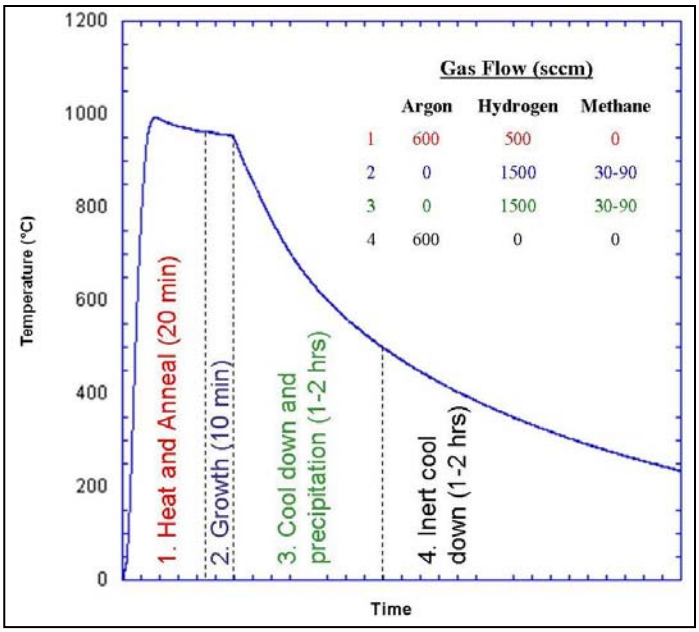

Figure 3. Reaction timeline detailing the CVD process for graphene and its different stages.

Characterization of these as-grown samples began with optical microscopy to identify the amount and relative thickness of deposition. Further imaging and identification was done with scanning electron microscopy (SEM). Raman spectroscopy (Renishaw inVia Raman Microscope, 633 nm laser, laser power output: ~15 mW, spot size: ~1 μm^2) was also performed to identify surface coverage and to characterize the deposited layers. Varying graphene layer thicknesses can also be discerned optically by the shade intensity of the area in question, with thin layers appearing lighter than thicker ones. We examined substrates with the optical microscope attached to the Raman microscope to find representative areas. An image of the area was then captured, and each area where Raman spectroscopic scans were performed was marked.

Note that AFM was not performed prior to transfer, since thickness measurements of the graphene on Ni would be difficult to quantify.

2.3 Transfer Process

Future device integration and more definitive characterization require the ability to transfer graphene thin films to different substrates. This procedure (see figure 4), began with spinning polymethyl methacrylate (MicroChem 495 PMMA A4) onto the surface of the substrate to form a thin coating. Optimal spin conditions were 4 s at 400 rpm, followed by 45 s at 4000 rpm, producing an ~2000 Å thick layer. This was followed by a soft bake at 185 °C for 1 min. Samples were then placed in a 6:1 buffered oxide etchant solution for 15 min to remove the SiO_2. Next, they were placed in a 1M $FeCl_3$ aqueous solution, acting as a nickel etchant. After several hours, the nickel was completely etched, leaving only the PMMA/graphene thin film which sticks to the bare silicon surface. After etching, the substrate was then transferred to water for rinsing. With a slight perturbation to the media or gentle tweezer manipulation, the visible thin film could then be released free-floating to the surface of the water. At this point, a different substrate was placed in the water underneath the floating thin film, and the PMMA/graphene layer adhered to the substrate surface. After allowing the wafer to dry, it was soaked with acetone to remove the PMMA, leaving the graphene layer remaining adhered to the surface due to van der Waals interactions. To remove excess PMMA residue, an additional anneal was performed at 400 °C for 1 hr in an Ar/H_2 environment (1700 sccm and 1900 sccm respectively). After transfer, additional optical microscopy and Raman spectroscopy were performed. Atomic force microscopy was also performed for more detailed surface measurements, accurate graphene thickness determination, and imagery.

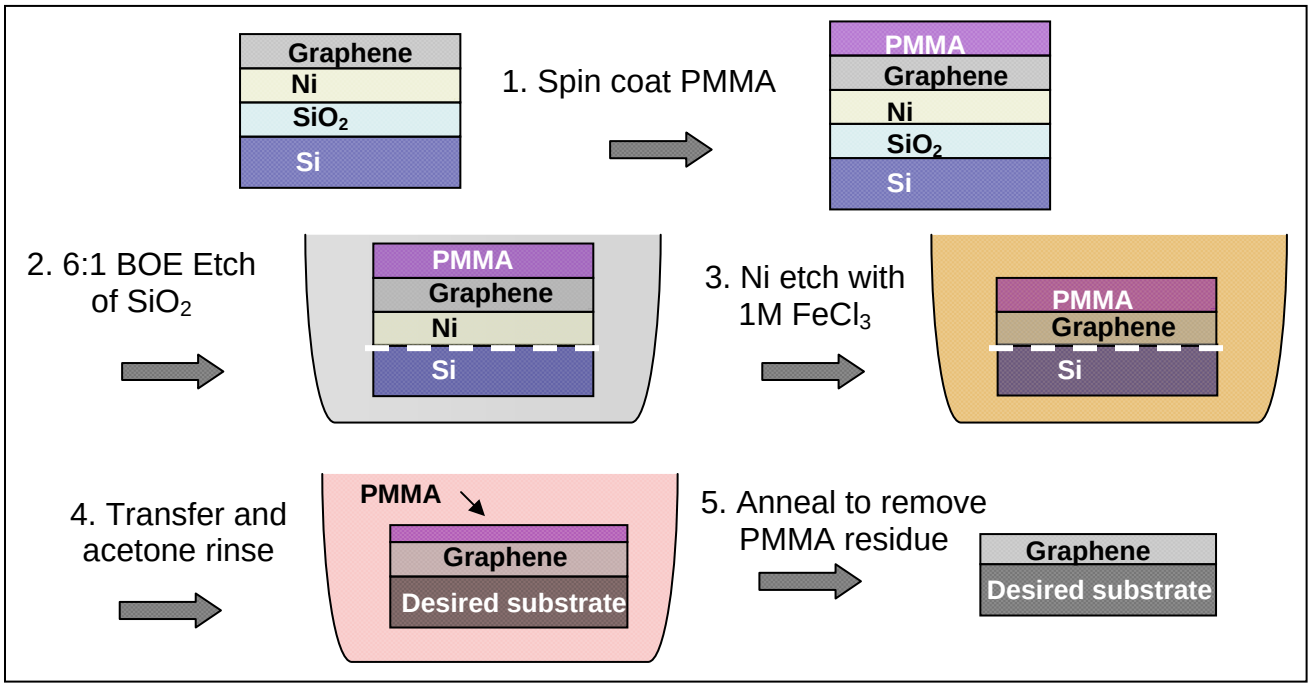

Figure 4. Step-by-step diagram of the transfer process for graphene thin films onto the desired substrate.

3. Results and Discussion

3.1 Effect of Annealing on Nickel Grain Size

Annealing was performed to facilitate development of the nickel surface as a template for graphene growth. It is generally thought that larger Ni grains will yield larger graphene flakes. Films were annealed as described in the experimental section. Results showed an increase in the average nickel grain size 40–50 times the original size. Surface roughness (σ_{RMS}) values increased as well, but this was largely a result of the dramatic differences in height due to the grain boundaries. Table 2 and figure 5 show this increase in grain size and surface roughness both quantitatively and qualitatively. AFM scans of the annealed nickel films with and without the chromium adhesion layer showed similar transformations and therefore indicate that the Cr layer did not influence nickel grain growth. These results show that annealing provides larger grains, but the process used holds room for improvement (i.e., longer anneal time). Nickel grain size and film uniformity are key factors in this process that should be examined further.

Table 2. AFM surface roughness and grain size measurements of nickel thin films pre- and post-anneal. Data was averaged from five scans per wafer at different locations to provide an accurate depiction of the topography throughout the sample.

Substrate	σ_{RMS} (nm)	R_a (nm)	Avg. Grain diameter (nm)
1 µm SiO_2	0.5	0.4	N/A
1000 Å Ni	1.5	1.2	40
2000 Å Ni	3.0	2.2	50
3000 Å Ni	3.5	2.8	45
1000 Å Ni (annealed at 1000 °C)	9.5	7.5	1500
2000 Å Ni (annealed at 1000 °C)	10.6	8.6	2000
3000 Å Ni (annealed at 1000 °C)	10.8	8.4	2000

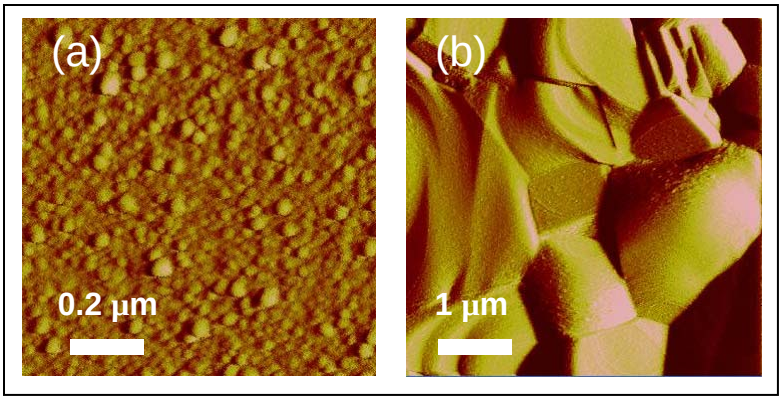

Figure 5. AFM deflection-error images of a 1000 Å nickel film (a) before and (b) after annealing.

3.2 Raman Spectroscopy on As-Grown Graphene Thin Films

Graphene's Raman spectrum is composed of three major peaks: (1) the D-band, centered at ~1328 cm^{-1}, is attributed to a disorder-induced first-order scattering (interlayer effects) (*21*); (2) the G-band at ~1583 cm^{-1} is a result of in-plane (intralayer) vibrations of the sp^2-hybridized carbon atoms; and (3) the 2D-band located around ~2700 cm^{-1} is an overtone of the D-band and can be attributed to a two phonon double resonance Raman process (*23*, *24*). Based on these characteristic peak positions and relative intensities, as well as optical color contrast, information about the number of layers can be determined. Figure 6 shows the Raman spectra from varying areas of growth on a 2000 Å nickel film.

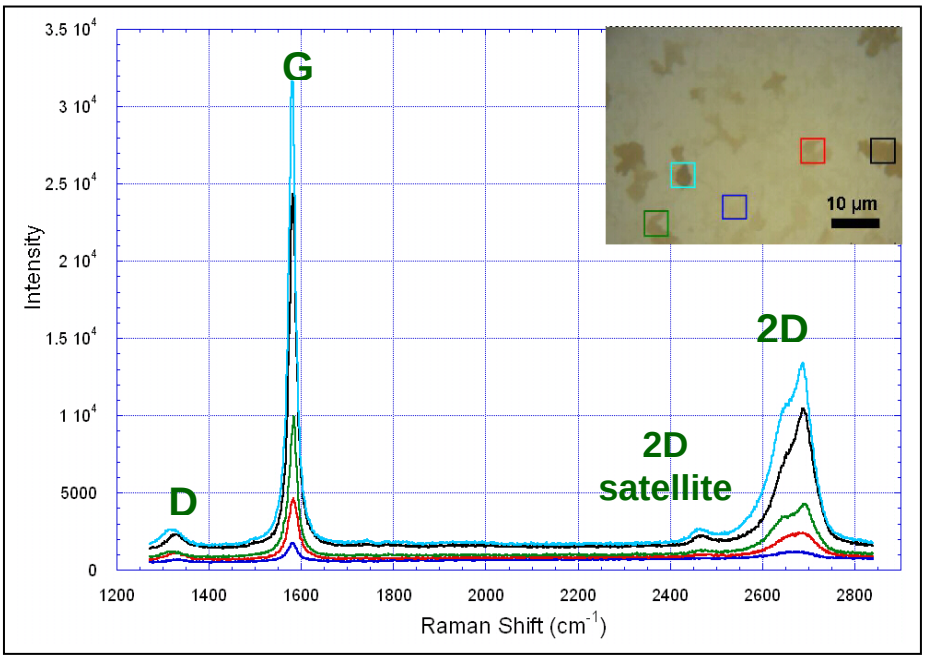

Figure 6. Raman spectra of five different areas of increasing shading and number of graphene layers, ranging from barren (blue) to multi-layer (black and neon blue) with important peaks identified. Areas are identified on the complimentary optical image and graph with corresponding colors.

With increasing number of layers, there is: (1) a greater overall signal intensity, (2) an emergence of a 2D satellite peak, and (3) a characteristic shape shift of the 2D peak. When comparing samples deposited under the same growth conditions, the overall signal intensity increased with the shading and number of layers. Since the G-band is attributed to intralayer effects, one would expect the intensity to scale with the number of layers and this is indeed found within the increase in overall signal intensity. Zero-layer, or areas absent of graphene growth, showed rather weak intensities assumed to be from surrounding deposition and were therefore deemed barren. Greater prominence of the 2D satellite peak, centered around 2465 cm^{-1} from single- to multi-layer deposition, allows further ability to discern these areas. When the two previous trends are combined with the characteristic 2D shape shift, they together paint an accurate and helpful portrait of varying thicknesses of deposition. The 2D-band can be fit with

the addition of two Lorentzian curves with high regression values (as shown in figure 7), their relative intensities providing qualitative information about the layer thickness. As the layers increase from single- to multi-layer deposition, the second of these peaks (~2697 cm^{-1}) begins to outweigh the first (~2655 cm^{-1}), dramatically altering the shape and providing a distinct Raman signature for the corresponding optical image. Note that the 2D-band actually contains four components, but for purposes of accentuating the two main peaks, this should suffice.

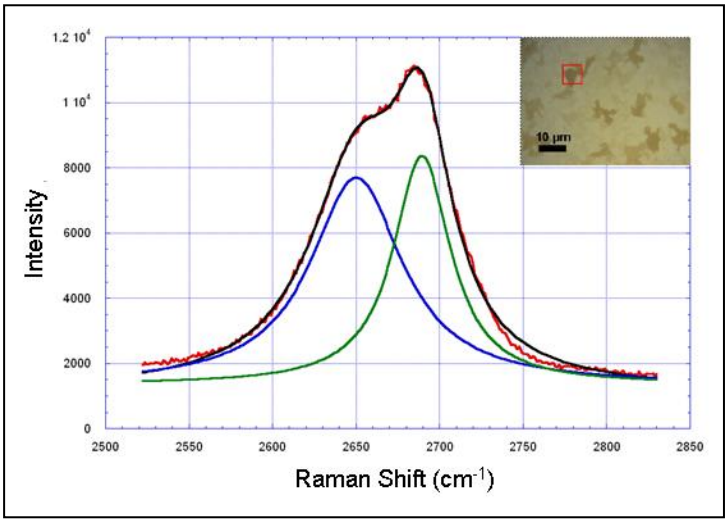

Figure 7. Double-Lorentzian fit of typical few- to multi-layer area emphasizing two peak composition. Constituent peaks are centered at ~2655 cm^{-1} with a full width at half maximum of 40 cm^{-1} and 2697 cm^{-1} with a full width at half maximum of 20 cm^{-1}.

A different set of characteristics, more definitive than the previous, are used to further distinguish between few-layer and heavy multi-layer to graphitic areas (see figure 8). Paramount among these characteristics is the relative intensity of the G- and 2D-bands (I_G/I_{2D}). This ratio is greater than one for few-layer deposition ($I_G>I_{2D}$) and less than one for the multi-layer graphene ($I_G<I_{2D}$). With the 2D-band representing second-order disorder-related effects, more layers would indicate greater occurrence of these interlayer disorder-related events and therefore an enhanced 2D signal. Since the D-band is also influenced by the disorder accompanied by increasing graphene thickness, there should be a greater relative height of the D-band. This was generally found to be true. Inconsistencies could be attributed to disparities in Raman laser position with measurements incorporating more graphene flake edges than expected, inherently containing more defects and making comparison difficult.

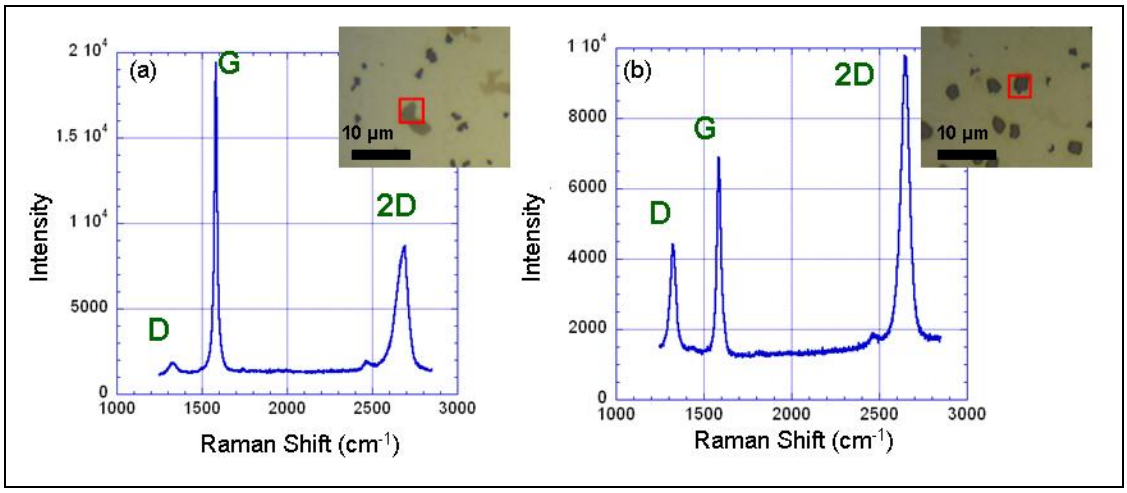

Figure 8. Shift in relative intensity of the G and 2D peaks between (a) a medium-shaded, few-layer area and (b) a dark-shaded, multi-layer graphene or graphite area. Corresponding optical images are shown.

Dark-shaded locations were not only distinct and easily distinguishable from surrounding deposition optically, but they had several characteristic Raman signatures unique to them, as demonstrated in figure 8. While this allows the ability to discern between relative shading intensities, it does not conclusively indicate the graphene layer thickness. Insight can be gained when the Raman spectra of CVD synthesized graphite is used as a reference for comparison. Prominent peak positions and relative intensities are nearly indistinguishable between the two samples (see figure 9). Results would therefore imply that these dark-shaded areas indeed fall in the range of heavy multi-layer graphene (greater than 10 layers) to graphite. It is noted that the Raman spectrum of HOPG, highly researched and publicized, differs from that observed from CVD-grown graphite (*25*).

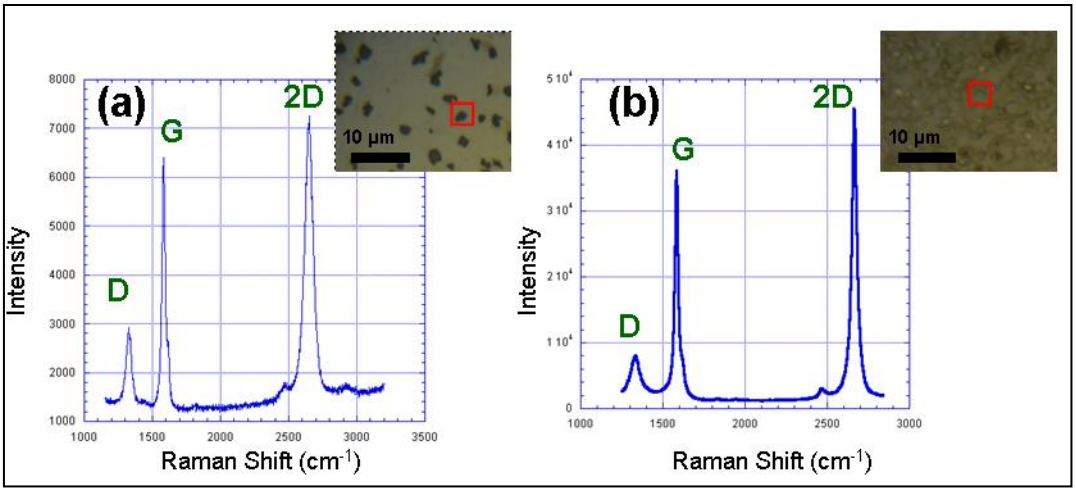

Figure 9. Comparison of Raman spectra of (a) a dark-shaded area and (b) graphite, both grown via chemical vapor deposition. Insets show an optical image of the area inspected.

3.3 Patterns in Growth Conditions

After investigating the selected growth parameters, several trends emerged. Cooling rate, acting as a means of controlling the extent and rate of carbon precipitation, was the most important variable in improving graphene film surface coverage. A decrease in the cooling rate from 25 to 5 °C was advantageous to producing continuous graphene thin films (see figure 10a). While greater overall coverage was achieved, an increased proportion of the film resulted with additional layer growth.

Increasing the nickel film thickness also seemed to have similar effects (see figure 10b). For the 1000 Å thick sample, barren and graphitic areas were more numerous than found for the 2000 Å and 3000 Å thick Ni films. As the Ni thickness increased, not only did the surface coverage increase, but the films produced were comprised of significantly more single- to few-layer depositions than multi-layer films. This development most likely result from an increased solubility of the thicker Ni films, which not only raises the probability of deposition, but also the extent.

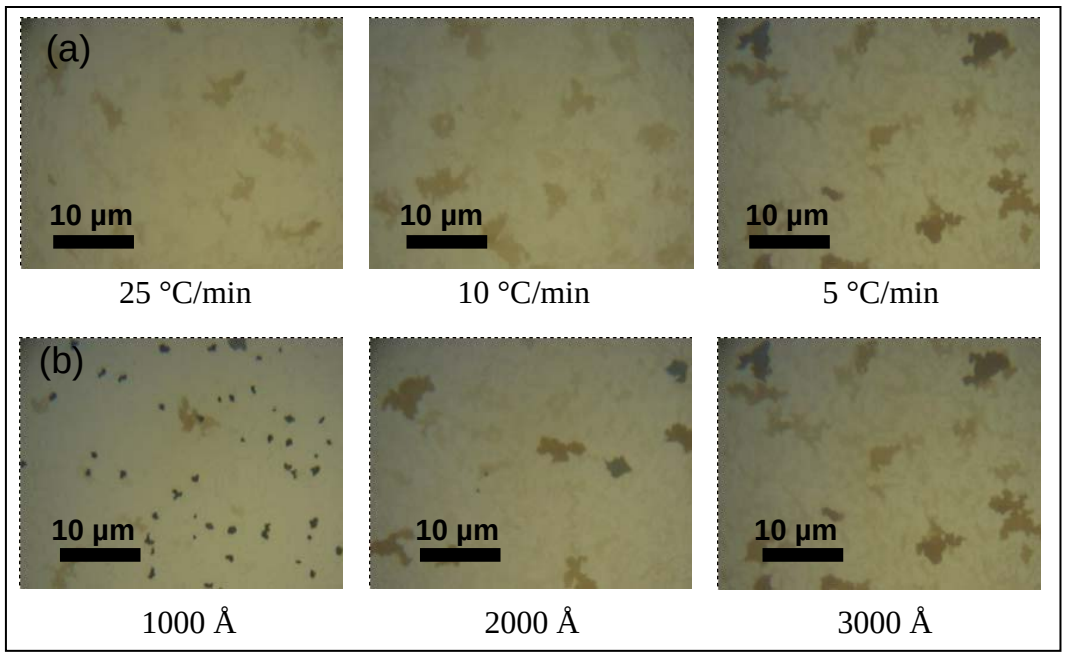

Figure 10. Trends in CVD synthesis conditions, with (a) decreased cooling rates and (b) increased nickel thicknesses. Both exhibit increased continuity and surface coverage, while the latter highlights the transition from graphite to graphene. All reactions performed at 900 °C and 60 sccm of methane.

Methane flow rate, providing the carbon source for graphene growth, exhibited both a temperature and nickel thickness dependence for producing optimal conditions. For example, an insufficient methane flow to generate deposition at one temperature (30 sccm at 900 °C), produced far more desirable results at an increased temperature (1000 °C). Thus, flow rates

should be tailored to the selection of other growth parameters (i.e., temperature, nickel thickness, cooling rate).

Additionally, temperature effects yielded inconclusive results, underscoring the interdependence of certain growth variables. While the type of deposition differed little between the two temperatures examined, note that the 1000 °C depositions showed greater inconsistency. This inconsistency included the appearance of areas completely void of deposition and apparent "burn marks," where the nickel film had given way to the silicon dioxide surface below. For future applications desiring continuous graphene sheets, 1000 °C may be too elevated of a temperature for reliable growth.

3.4 Characterization on Transferred Films

After many trials, up to 80% of the as-grown graphene film was able to be effectively removed and placed on a 300 nm SiO_2/Si wafer with the transfer method developed (see figure 4 for review). Room for significant improvement exists; however, for characterization purposes, this is more than sufficient. Transfer to this substrate is an important achievement not only as a proof-of-principle demonstration, but also for optical contrast methods and atomic force microscopy measurements to identify varying numbers of graphene layers. Even simpler, it allows a far more accurate assessment of the overall surface coverage, which is significantly more visible than graphene films against the Ni catalyst layer (see figure 11).

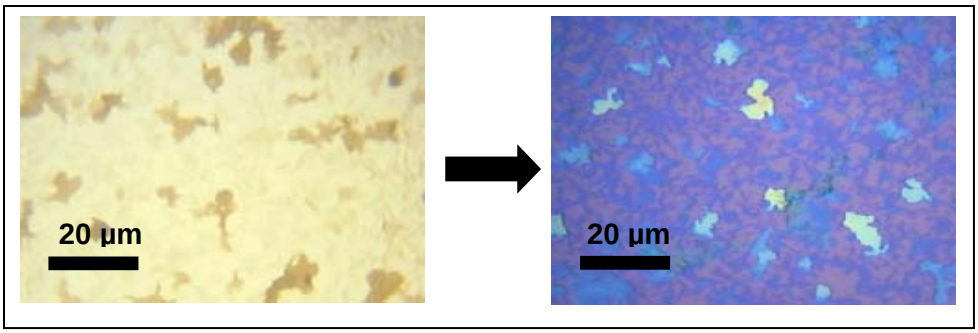

Figure 11. Optical image comparison of graphene thin films as-grown (left) and after undergoing transfer to a 300 nm SiO_2/Si wafer (right). While graphene flakes are evident on both substrates, deposition is easily discerned in the latter with the bare SiO_2 (seen as light purple) visible beneath.

Raman spectroscopy was performed on the transferred films to confirm observations made on the previously measured graphene on nickel samples. Trends found prior to transfer were still evident with an accompanied increase in signal intensity. AFM was also performed on transferred graphene films to obtain a better understanding of the topography as well as to confirm thicknesses. Wrinkles formed either during growth or during the transfer process were imaged, as shown in figure 12a. Surface roughness measurements of the graphene surface are well under 1 nm. Measuring the relative height changes between adjacent flakes (see figure 12b) confirms integer-based increases of roughly 0.35 nm in agreement with previously reported results (*19, 21*). Height measurements were inconclusive due to high surface roughness values

of the underlying SiO_2 layer. (Although 300 nm thermally oxided silicon substrates are preferred due to their low surface roughness, these substrates were unavailable at the time of experimentation). These difficulties obtaining accurate height measurements must be remedied to verify graphene layer thickness with optical contrast observations.

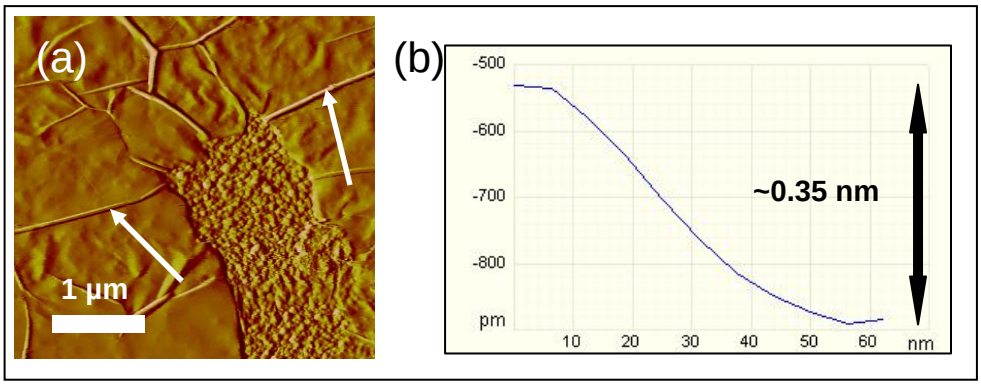

Figure 12. (a) AFM deflection-error image of a graphene thin film transferred onto a 300 nm SiO_2/Si wafer prepared by plasma enhanced chemical vapor deposition. Bare SiO_2 surface visible next to surrounding graphene flakes; wrinkles are denoted by arrows. (b) AFM height measurement across a wrinkle confirming interlayer spacing of ~0.35 nm.

4. Conclusion

Procedures for growth via chemical vapor deposition, transfer, and characterization of large-area, single- to few- and multi-layer graphene sheets were established. Slower cooling rates and increased nickel thickness yielded greater surface coverage, as well as increasing the number of layers at many areas. Color contrast using optical microscopy and Raman spectroscopy identified trends to aid in distinguishing the relative number of layers. Relative intensities, shapes, and positions of characteristic graphene-related peaks produced distinct Raman spectra for identifying composition. The transfer process, while sufficient for research purposes, can be further developed to increase yields. Further information can be obtained through atomic force microscopy measurements and additional optical microscopy imaging. The trends discovered here should provide direction for future optimization of the CVD process. Results suggest that further improvement can be made by increasing the nickel film grain size and uniformity.

5. References

1. Novoselov, K. S.; et al. *Science* **2004**, *306*, 666–669.
2. Geim, A. K.; Novoselov, K. S. *Nature Materials* **2007**, *6*, 183–191.
3. Castro Neto, A. H.; et al. *Reviews of Modern Physics* **2009**, *81*, 109–162.
4. Novoselov, K. S.; et al. *Nature* **2005**, *438*, 197–200.
5. Jia, X.; et al. *Science* **2009**, *323*, 1701–1705.
6. Hwang, E. H.; et al. *Physical Review Letters* **2007**, *98* 186806-1–186806-4.
7. Geim, A. K. *Science* **2009**, *324*, 1530–1534.
8. Ponomarenko, L.A.; et al. *Science* **2008**, *320*, 356–358.
9. Westervelt, R. M. *Science* **2008**, *320*, 324–325.
10. Kane, C. L. *Nature* **2005**, *438*, 168–170.
11. Schedin, F.; et al. *Nature Materials* **2007**, *6*, 652–655.
12. Elias, D. C.; et al. *Science* **2009**, *323*, 610–613.
13. Lee, C.; et al. *Science* **2008**, *321*, 385–388.
14. Balandin, A. A.; et al. *Nano Letters* **2008**, *8* (3), 902–907.
15. Reina, A.; et al. *Nano Letters* **2009**, *9* (1), 30–35.
16. Kim, K. S.; et al. *Nature* **2009**, *457*, 706–710.
17. Arco, L.G.D.; et al. *IEEE Transactions on Nanotechnology* **2009**, *8* (2), 135–138.
18. Chae, S. J.; et al. *Advanced Materials* **2009**, *21*, 1–6.
19. Reina, A.; et al. *Nano Res.* **2009**, *2*, 509–516.
20. Li, X.; et al. *Science* **2009**, *324*, 1312–1314.
21. Gupta, A.; et al. *Nano Letters* **2006**, *6* (12), 2667–2673.
22. Kajihara, M.; Hillert, M. *Metall. Trans. A* **1990**, *21* (10), 2777–2787.
23. Ni, Z.; et al. *Nano Res.* **2008**, *1*, 273–291.
24. Park, J.S.; et al. *Carbon* **2009**, *47*, 1303–1310.
25. Obraztsov, A. N.; et al. *Carbon* **2008**, *46*, 963–968.

NO. OF COPIES	ORGANIZATION
1 ELEC	ADMNSTR DEFNS TECHL INFO CTR ATTN DTIC OCP 8725 JOHN J KINGMAN RD STE 0944 FT BELVOIR VA 22060-6218
1	DARPA ATTN IXO S WELBY 3701 N FAIRFAX DR ARLINGTON VA 22203-1714
1 CD	OFC OF THE SECY OF DEFNS ATTN ODDRE (R&AT) THE PENTAGON WASHINGTON DC 20301-3080
1	US ARMY RSRCH DEV AND ENGRG CMND ARMAMENT RSRCH DEV AND ENGRG CTR ARMAMENT ENGRG AND TECHNLGY CTR ATTN AMSRD AAR AEF T J MATTS BLDG 305 ABERDEEN PROVING GROUND MD 21005-5001
1	PM TIMS, PROFILER (MMS-P) AN/TMQ-52 ATTN B GRIFFIES BUILDING 563 FT MONMOUTH NJ 07703
1	US ARMY INFO SYS ENGRG CMND ATTN AMSEL IE TD A RIVERA FT HUACHUCA AZ 85613-5300
1	COMMANDER US ARMY RDECOM ATTN AMSRD AMR W C MCCORKLE 5400 FOWLER RD REDSTONE ARSENAL AL 35898-5000
1	US GOVERNMENT PRINT OFF DEPOSITORY RECEIVING SECTION ATTN MAIL STOP IDAD J TATE 732 NORTH CAPITOL ST NW WASHINGTON DC 20402

NO. OF COPIES	ORGANIZATION
1	MATTHEW O'BRIEN 15300 37TH AVE NORTH #A318 PLYMOUTH, MN 55446
1	US ARMY RSRCH LAB ATTN RDRL CIM G T LANDFRIED BLDG 4600 ABERDEEN PROVING GROUND MD 21005-5066
9	US ARMY RSRCH LAB ATTN RDRL SER L M O'BRIEN ATTN IMNE ALC HRR MAIL & RECORDS MGMT ATTN RDRL CIM L TECHL LIB ATTN RDRL CIM P TECHL PUB ATTN RDRL SER P AMIRTHARAJ ATTN RDRL SER L B NICHOLS ATTN RDRL SER L B PIEKARSKI ATTN RDRL SER L M DUBEY ATTN RDRL SER L S KILPATRICK ADELPHI MD 20783-1197

TOTAL: 19 (1 ELEC, 1 CD, 17 HCS)

INTENTIONALLY LEFT BLANK.